

Nucleon Excited States in $N_f=2$ lattice QCD

C. Alexandrou,^{1,2} T. Korzec,³ G. Koutsou,² and T. Leontiou⁴

¹*Department of Physics, University of Cyprus, P.O. Box 20537, 1678 Nicosia, Cyprus*

²*The Cyprus Institute, P.O. Box 27456, 1645 Nicosia, Cyprus*

³*Institut für Physik, Humboldt Universität zu Berlin, Newtonstrasse 15, 12489 Berlin, Germany*

⁴*General Department, Frederick University, 1036 Nicosia, Cyprus*

We investigate the excited states of the nucleon using $N_f = 2$ twisted mass gauge configurations with pion masses in the range of about 270 MeV to 450 MeV and one ensemble of $N_f = 2$ Clover fermions at almost physical pion mass. We use two different sets of variational bases and study the resulting generalized eigenvalue problem. We present results for the two lowest positive and negative parity states.

I. INTRODUCTION

Understanding the excitation spectrum of hadrons, including that of the proton is still a challenge. In particular, the $P_{11}(1440\text{MeV})$ positive parity resonance known as the Roper, still remains a puzzle having a mass lower than the negative parity state $S_{11}(1535\text{MeV})$. This ordering is contrary to the prediction of constituent quark models where the negative parity state is lower in mass than P_{11} . Lattice QCD simulations have recently reproduced the mass of the low-lying baryon states using gauge configurations with pions having mass close to the physical value [1, 2]. In these studies volume and cut-off effects have been taken into account by performing the calculation at different volumes and lattice spacings. Contrary to the low-lying baryon states the study of excited states has not yet reached the same level of maturity. In order to extract excited state energies, a robust analysis of simulation data keeping systematic errors under control is needed.

The study of excited states is mostly based on the variational principle, which was first applied to extract glueball masses [3]. One considers a number of interpolating fields as a variational basis and a generalized eigenvalue problem (GEVP) is defined, which yields the low-lying energy levels. The GEVP has been applied recently to study hadron spectroscopy by a number of lattice groups [4–8]. A crucial question of such an approach is the convergence of the energy levels to the true value. This was first addressed in a paper by Lüscher and Wolff [9] and recently by the ALPHA-collaboration [10]. In this work, we explore the variational approach as put forward by the ALPHA-collaboration to study the excited states of the nucleon in the positive and negative parity channels. We examine two types of nucleon interpolating fields as well as different levels of Gaussian smearings. The approach proposed by the ALPHA-collaboration is compared with the standard GEVP, where the reference time t_0 is kept fixed at a small value. The main outcome of this comparison is that, within the current statistical accuracy typically used for baryon calculations, namely $\mathcal{O}(10^2)$ configurations, we do not see any improvements to the standard analysis. Having established at one ensemble of twisted mass fermions that

the standard generalized eigenvalue approach performs equally well, we adopt it for the other ensembles. In the positive parity channel we include in the variational basis interpolating fields with a large and small number of iterations in the Gaussian smearing. This is crucial to reproduce a state with lower energy closer to the Roper state. As argued in Refs. [7, 11, 12] a linear combination of interpolating fields corresponding to a small and large root mean square radius (rms) produces a wavefunction with a node having potentially a larger overlap with the Roper state. We indeed observe a lowering in the energy of the first excited state when including an interpolating field with a large rms radius.

We analyze a total of five ensembles of $N_f = 2$ twisted mass fermions with pion mass in the range of about 270 MeV to 450 MeV and lattice spacing $a = 0.089$ fm determined from the nucleon mass [2]. Cut-off effects on the mass of the nucleon and hyperons were examined in Refs. [2, 13] respectively using, in addition to the one used here, two smaller lattice spacings. The conclusion was that cut-off effects were within the statistical errors and one could take the continuum limit assuming negligible $\mathcal{O}(a^2)$ effects. Therefore, in this work, we limit ourselves to studying only one lattice spacing. In addition, we analyze an ensemble of $N_f = 2$ Clover fermions with pion mass $m_\pi \sim 160$ MeV and lattice spacing $a \simeq 0.073$ fm.

The paper is organized as follows: In section II we give the details of the simulations, in section III we compare results using different variational bases and analysis approaches using an ensemble of twisted mass fermions with $m_\pi \sim 300$ MeV, in section IV we give our results and in section V we summarize our findings and give our conclusions.

II. SIMULATION DETAILS

The input parameters of the calculation using $N_f = 2$ twisted mass fermions, namely β , L/a and $a\mu$ are summarized in Table I. These are the same configurations already used in the analysis of the low-lying baryon spectrum [13], where more details regarding the twisted mass formulation can be found. The corresponding lattice spacing a and the pion mass values, spanning a mass

range from 270 MeV to 450 MeV, are taken from Ref. [2]. We note that for baryon masses we use the lattice spacing determined from the nucleon mass, which is consistent with the one extracted from f_π [14].

$\beta = 3.9, a = 0.089(1)(5)$ fm from the nucleon mass				
$r_0/a = 5.22(2)$				
$24^3 \times 48,$ $L = 2.05$ fm	$a\mu$	0.0040	0.0064	0.0085
	No. of confs	400	400	348
	m_{π^\pm} (GeV)	0.3131(16)	0.3903(9)	0.4470(12)
	Lm_{π^\pm}	3.25	4.05	4.63
$32^3 \times 64,$ $L = 2.74$ fm	$a\mu$	0.003	0.004	
	No. of confs	400	250	
	m_{π^\pm} (GeV)	0.2696(9)	0.3082(6)	
	Lm_{π^\pm}	3.74	4.28	

TABLE I. Input parameters (β, L, μ) of our lattice calculation and corresponding lattice spacing (a), pion mass (m_π) and number of gauge field configurations used. The values of the pion mass in physical units were obtained using the lattice spacing determined from f_π , namely $a = 0.0855(6)$ fm.

Apart from the twisted mass fermion ensembles given in Table I we also analyze an ensemble of $N_f = 2$ Clover fermion configurations produced by the QCDSF collaboration. We use the $48^3 \times 64$ ensemble with near-physical pion mass of $m_\pi \simeq 160$ MeV, at $\beta = 5.29$ for which the lattice spacing has been determined to be $a = 0.0728(5)(19)$ fm [15]. This yields a value for $Lm_\pi \simeq 2.8$. We smear the links that enter the Dirac operator with three iterations of APE smearing [16] to reduce gauge noise and set the clover term to its tree-level value i.e. $c_{SW} = 1$. Smearing the links in this way changes κ_{crit} . We therefore tune the value of the hopping parameter κ as described in [17] to match the pion mass in the unitary theory. A comparison of the pion and nucleon effective masses, $am_{\text{eff}}(t) \equiv C(t)/C(t+1)$, in the unitary theory and after tuning is shown in Fig. 1. As can be seen, the mass of the nucleon in the non-unitary theory agrees with the one obtained in the unitary theory. Note that one has to allow 10 time slices or about 0.7 fm to ensure that excited states have been sufficiently suppressed. This is a rather large time interval given that the mass gap between the ground and the excited state estimated from a double exponential fit, yields a suppression factor of $\mathcal{O}(e^{-4})$, which means that there is a substantial overlap of the standard nucleon interpolating field with higher excited states.

III. THE VARIATIONAL METHOD

The standard extraction of the ground state energy from the large time limit of Euclidean two-point correlation functions relies on the fact that they are expressed as a sum of the energy eigenstates of QCD that exponen-

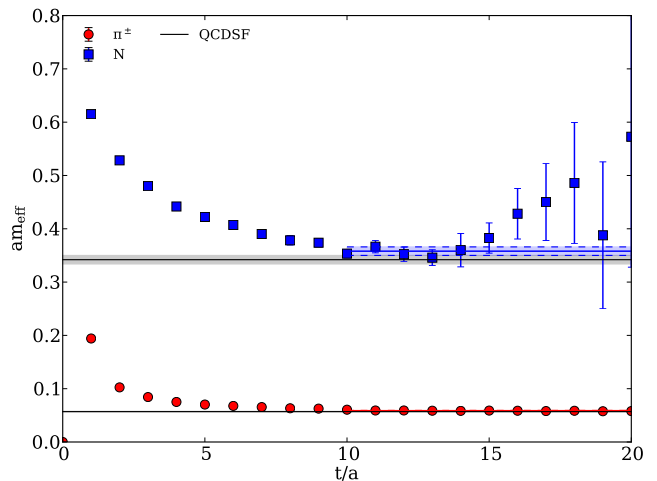


FIG. 1. The pion (red circles) and nucleon (blue squares) effective masses in the non-unitary setup as described in the text, compared to their values in the unitary theory (solid black line) computed by QCDSF [15]. The value of κ in the non-unitary setup was tuned to reproduce the pion mass in the unitary theory.

tially decay as a function of the time with a rate proportional to the energy. The variational method provides an approach for extracting, besides the lowest energy state, the low-lying excited states from Euclidean correlation functions. A variational basis is constructed by using different interpolating fields χ with the quantum numbers of the particular state of interest, which in this work is the nucleon. Applying the variational principle one can determine the superposition of states that correspond to the low-lying nucleon states. One variational basis is obtained by considering two different spin combinations of nucleon interpolating fields, namely

$$\chi_1 = (u^T C \gamma_5 d)u \quad \text{and} \quad \chi_2 = (u^T C d)\gamma_5 u. \quad (1)$$

The nucleon interpolator, χ_1 , is well known to have a good overlap with the ground state of the nucleon, while the χ_2 interpolator vanishes in the non-relativistic limit and thus has a small overlap with the nucleon ground state, which is a motivation to include it in a variational basis to study the excited states. In addition, the variational basis is enlarged by considering different Gaussian smearings using similar parameters to those used in Ref. [10], as well as an interpolating field with larger smearing, which maybe needed for isolating the Roper. The correlation matrix considered here, thus, has the

general form:

$$\begin{aligned}
C_{a_i b_j}^\pm(t) &= \sum_{\mathbf{x}} \text{Tr} \left[\frac{1}{4} (1 \pm \gamma_0) \langle \chi_a^{(i)}(\mathbf{x}, t) \bar{\chi}_b^{(j)}(\mathbf{0}, 0) \rangle \right] \\
&= \sum_{n=0}^{\infty} e^{-E_n t} \text{Tr} \left[\frac{1}{4} (1 \pm \gamma_0) \langle 0 | \chi_a^{(i)} | n \rangle \langle n | \chi_b^{(j)} | 0 \rangle \right], \\
&i, j = 1, \dots, N \\
&a, b = 1, 2,
\end{aligned} \tag{2}$$

where the trace is taken over Dirac indices and $C^+(t)$ ($C^-(t)$) yields the positive (negative) parity correlator [18]. The states $|n\rangle$ are eigenstates of the Hamiltonian with $E_n < E_{n+1}$ and we have assumed that the temporal extent of the lattice is large enough to neglect contributions due to the finite size of the temporal direction. The indices i and j on the correlation matrix $C^\pm(t)$ correspond to different levels of Gaussian smearing and a and b to χ_1 and χ_2 .

A. Variational basis with different gaussian smearing levels of χ_1

In this subsection, we perform an analysis using as a variational basis χ_1 with a number of different smearing levels. The variational basis is constructed using N different Gaussian smearing levels of this interpolating field. The GEVP is defined by the generalized eigen-equation

$$\begin{aligned}
C(t)v_n(t, t_0) &= \lambda_n(t, t_0)C(t_0)v_n(t, t_0), \\
n &= 1, \dots, N, t > t_0,
\end{aligned} \tag{3}$$

where $E_n = \lim_{t \rightarrow \infty} -\partial_t \log \lambda_n(t, t_0)$. The corrections to E_n decrease exponentially like $e^{-\Delta E_n t}$ where $\Delta E_n = \min_{m \neq n} |E_m - E_n|$ [9] for fixed t_0 . In Ref. [9, 10] it was shown that if one varies t_0 such that $t_0 \geq t/2$ then the correction is $\mathcal{O}(e^{-\Delta E_{n,n} t})$ with $\Delta E_{m,n} = E_m - E_n$ ensuring a greater rate of convergence. In this section, we examine the benefit of this relation for extracting the low-lying states in the nucleon sector. A related work exploring the dependence of the GEVP on the reference time is also examined in Ref. [19] where recurrence relations are obtained. The variational method has also been extensively used to study the excited nucleon spectrum by the Berlin-Graz-Regensburg (BGR) collaboration [20].

We apply Gaussian smearing to each quark field, $q(\mathbf{x}, t)$ [21, 22], entering χ_1 . The smeared quark field is given by $q^{\text{smeared}}(\mathbf{x}, t) = \sum_{\mathbf{y}} F(\mathbf{x}, \mathbf{y}; U(t))q(\mathbf{y}, t)$ using the gauge invariant smearing function

$$F(\mathbf{x}, \mathbf{y}; U(t)) = (1 + \alpha H)^{n_s}(\mathbf{x}, \mathbf{y}; U(t)), \tag{4}$$

constructed from the hopping matrix understood as a matrix in coordinate and color space

$$H(\mathbf{x}, \mathbf{y}; U(t)) = \sum_{i=1}^3 \left(U_i(\mathbf{x}, t) \delta_{\mathbf{x}, \mathbf{y} - a\hat{i}} + U_i^\dagger(\mathbf{x} - a\hat{i}, t) \delta_{\mathbf{x}, \mathbf{y} + a\hat{i}} \right). \tag{5}$$

Smearing is applied at the fermion source and sink. Following Ref. [10] we consider values of the smearing parameters $\alpha = 0.1$ and $n_s = 0, 22, 45, 67$ and 135. These smearing parameters produce a source with a root mean square radius in lattice units of 0, 1.96, 2.72, 3.25 and 4.48, respectively. These different smearing levels are labeled by the superscript $i = 1, \dots, 5$ on $\chi^{(i)}$. We will refer to this basis as *basis A*. The resulting correlation matrices are symmetrized. We use 150 twisted mass configurations with $\beta=3.9$, $a\mu = 0.004$ or $m_\pi \sim 308$ MeV on a $32^3 \times 64$ lattice. In addition, we also construct a 3×3 GEVP with a variational basis that includes a heavily smeared interpolating field. For the latter basis, referred to as *basis B*, the values of the smearing parameters are $\alpha = 4.0$ and $n_s = 10, 50, 180$ producing a source with rms radius in lattice units of 2.36, 4.87 and 8.60. We analyze 200 configurations of the same ensemble for this variational basis. These smearing levels will be labeled by the superscript $i = 6, 7$ and 8 on $\chi^{(i)}$. Although the rms for $i=6$ and $i=7$ is similar to $i=1$ and $i=5$ this new set contains the heavily smeared basis, $i=8$.

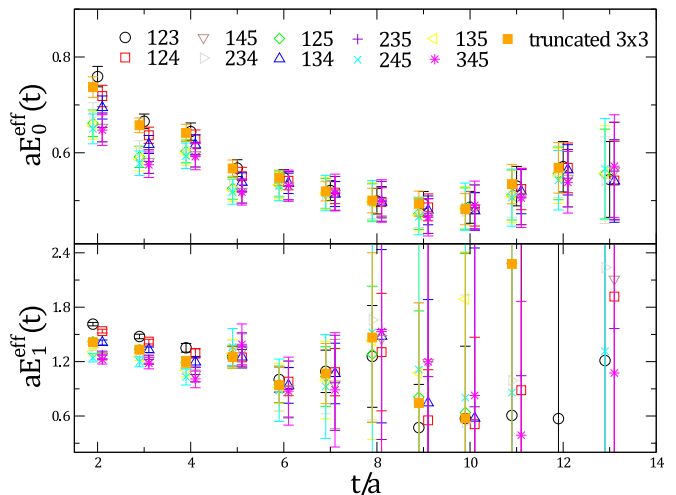


FIG. 2. The effective mass for the ground (E_0) and first excited (E_1) states resulting from a 3×3 GEVP using *basis A*. A 3×3 correlation matrix was constructed out of different interpolating fields $\chi_1^{(i)}$ by applying a different number of Gaussian smearing iterations on χ_1 . The numbers in the legend give the combination of the three values of n_s used to construct the basis. The effective energy levels resulting from a truncated 3×3 GEVP constructed using Eq. (6) are also shown. This analysis was carried out using 150 configurations of twisted mass fermions at $\beta=3.9$, $a\mu = 0.004$ ($m_\pi \sim 308$ MeV) on a $32^3 \times 64$ lattice.

Let us first examine the role of t_0 and the advantage of using these different smearing levels. We consider several different correlation matrices of the positive parity correlator $C_{1_1 1_j}^+(t)$ constructed from $\chi_1^{(i)}$ for different smearing levels $i = 1, \dots, 5$ in order to examine both the role of varying n_s and/or the dimensionality of the GEVP. In Fig. 2 we show the effective mass for the ground and first excited states resulting from a GEVP analysis of all pos-

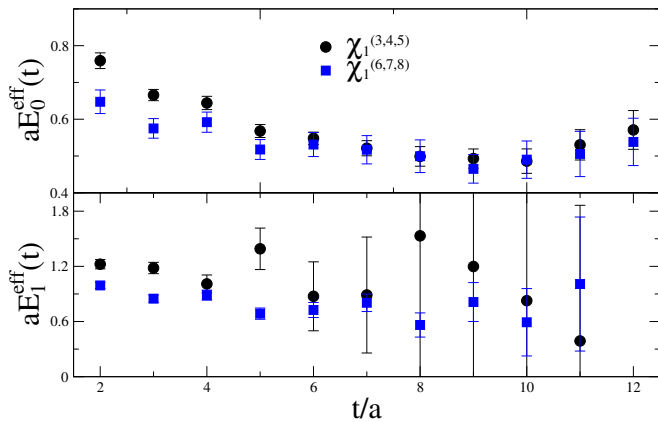


FIG. 3. The effective mass for the ground (E_0) and first excited (E_1) states resulting from a 3×3 GEVP using *basis A* (interpolating fields $\chi_1^{(3)}$, $\chi_1^{(4)}$ and $\chi_1^{(5)}$) using 150 gauge configurations (black filled circles) and *basis B* using 200 gauge configurations (blue filled squares) of twisted mass fermions at $\beta=3.9$, $a\mu = 0.004$ ($m_\pi \sim 308$ MeV) on a $32^3 \times 64$ lattice.

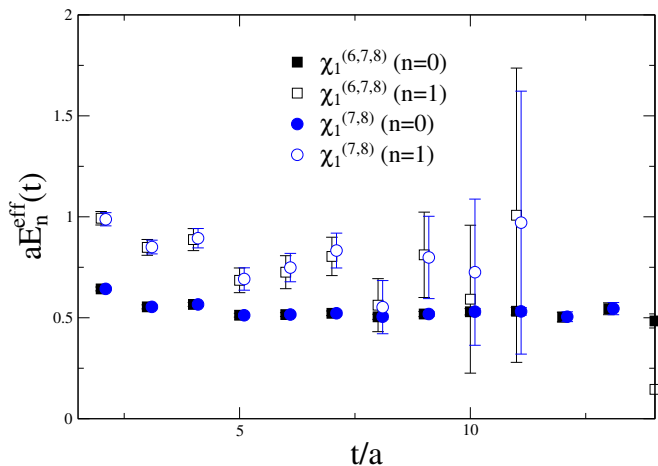


FIG. 4. The effective mass for the ground and first excited states from the best choice of 2×2 and 3×3 GEVPs corresponding to the highest level of Gaussian smearing i.e. from $\{\chi_1^{(7)}, \chi_1^{(8)}\}$ for the 2×2 GEVP and $\{\chi_1^{(6)}, \chi_1^{(7)}, \chi_1^{(8)}\}$ for the 3×3 GEVP. The test was carried out using 200 configurations of the twisted mass ensemble with $\beta=3.9$, $a\mu = 0.004$ ($m_\pi \sim 308$ MeV) on a $32^3 \times 64$ lattice

sible 3×3 correlation matrices fixing $t_0/a = 1$. We are looking for the combination of interpolating fields that gives the fastest convergence to the two-lowest levels E_0 and E_1 i.e. to the earliest onset of a plateau behavior. From this analysis it is evident that using the higher smearing levels improves convergence allowing us to fit to a constant starting from time-slice $t/a = 5$ for the ground state and from time-slice $t/a = 4$ for the first excited state. The condition number of this 3×3 GEVP ranges from 10^4 (when $\chi_1^{(1)}$, $\chi_1^{(2)}$ and $\chi_1^{(3)}$ are used) up to 10^6 (when $\chi_1^{(1)}$, $\chi_1^{(3)}$ and $\chi_1^{(5)}$ are used).

Next we examine the role of increasing the level of

smearing and compare the results obtained from the above analysis with a 3×3 GEVP using *basis B*. In Fig. 3 we show the effective mass for the ground and first excited states resulting from a 3×3 GEVP for both *basis A* and *basis B*. Using *basis B* we observe faster convergence to ground state and a lowering in the value of the excited state mass. The condition number for *basis B* is in the order of 10^6 . Furthermore, increasing the level of smearing beyond $n_s = 180$ does not result in any further lowering of the energy of the excited state but only leads to larger statistical errors. In fact the condition number of the correlation matrix gets worse increasing rapidly to $\mathcal{O}(10^9)$ when we use $n_s = 300$. The comparison of these results indicates that for the study of the positive parity states *basis B* is more suitable than *basis A*.

Apart from making a choice of the appropriate basis by trying different combinations of Gaussian smearing we also try a truncation scheme where the 5×5 correlation matrix is projected to an $m \times m$ matrix, $C^{m \times m}(t)$, with $m < N$ by using the $m < 5$ eigenvectors belonging to the m largest eigenvalues of $C(t_0)$ as follows

$$C^{N \times N}(t_0)b = \Lambda b, \quad C_{kj}^{m \times m}(t) = b_{ki}^\dagger C_{i_1 i_2}^{N \times N}(t) b_{i_2 j},$$

$$k, j = 1, \dots, m, \quad i_1, i_2 = 1, \dots, N, \quad (6)$$

where $\Lambda_{jk} = \delta_{jk} e^{-E_j t_0}$ is an $N \times N$ matrix with the eigenvalues of $C^{N \times N}(t_0)$ as its diagonal elements and b an $N \times N$ matrix with the corresponding eigenvectors. We additionally tried this truncation scheme with various values of t_0/a , namely $t_0/a = 1, \dots, 4$ and the results obtained are found to be statistically equivalent. The resulting effective masses extracted from the truncated 3×3 matrix using *basis A* are included in Fig. 2 and do not show any improved convergence.

The effect of reducing the dimension of the GEVP to 2×2 can be seen in Fig. 4. The quality of the plateaus for the first two states is not affected as compared to those extracted using the 3×3 correlation matrix with $\chi_1^{(6)}$, $\chi_1^{(7)}$ and $\chi_1^{(8)}$.

In Fig. 5 we compare the results obtained using the GEVP analysis to those extracted using a single interpolating field $\chi_1^{(i)}$, i.e. the trivial 1×1 GEVP. For the ground state, using just the $\chi_1^{(8)}$ interpolating field yields the same quality plateau as that obtained from the 3×3 correlation matrix analysis within *basis B*.

For the two lowest states in the positive channel we also study the resulting eigenvectors in order to understand/verify the mixture of the various $\chi_1^{(i)}$ contributing in the optimized interpolating field for each state. Identifying the optimum combination of $\chi_1^{(i)}$ extracted from the GEVP analysis is useful if one wants to calculate the matrix elements of any operator using the optimal interpolating field that best suppresses the contribution of excited states.

In Fig. 6 we show the three components V_1, V_2 and V_3 of the eigenvector for the ground and excited state in the positive parity channel determined from the 3×3

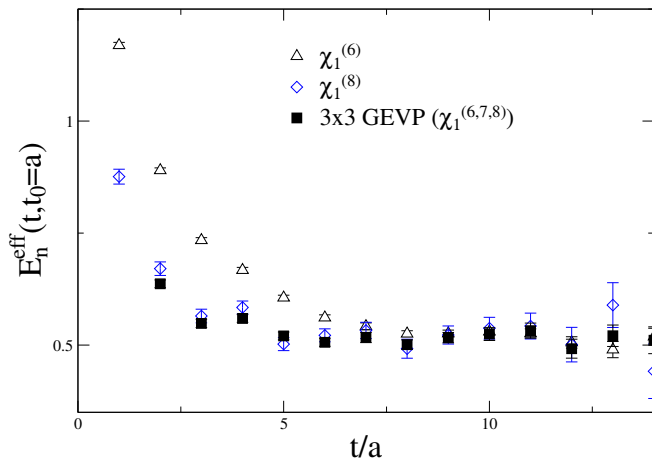


FIG. 5. The effective mass for the ground state for $t_0/a = 1$. Results shown are extracted from the GEVP with *basis B* and from the correlators $C_{1_6 1_6}$ and $C_{1_8 1_8}$.

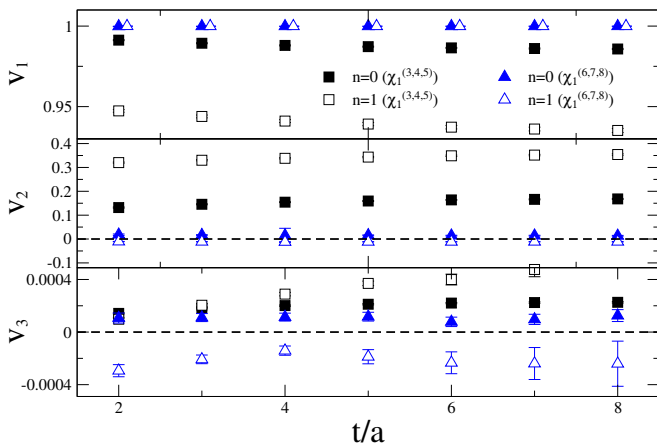


FIG. 6. The components of the eigenvector for the ground and first excited states at $t_0/a = 1$. The results are extracted from GEVP analyses of the 3×3 correlation matrices $C_{1_i 1_j}$, $i, j = 3, 4, 5$ and $C_{1_i 1_j}$, $i, j = 6, 7, 8$ (*basis B*).

correlation matrix for *basis A* (interpolating fields $\chi_1^{(3)}$, $\chi_1^{(4)}$ and $\chi_1^{(5)}$) and for *basis B* (interpolating fields $\chi_1^{(6)}$, $\chi_1^{(7)}$ and $\chi_1^{(8)}$). The interpolating field with the maximum overlap with the ground state is given by $\chi_{\text{eff}} = \tilde{v}_1 \chi_1^{(5)} + \tilde{v}_2 \chi_1^{(4)} + \tilde{v}_3 \chi_1^{(3)}$, or equivalently by $\chi_{\text{eff}} = \tilde{v}_1 \chi_1^{(8)} + \tilde{v}_2 \chi_1^{(7)} + \tilde{v}_3 \chi_1^{(6)}$, where \tilde{v} is the large-time limit of V i.e. $\tilde{v}(t_0) = \lim_{t \rightarrow \infty} V(t, t_0)$. It is evident that in the case of *basis B* one of the eigenvector component enters in with the opposite sign from the other two thus providing the possibility for a nodal structure, not possible with *basis A*. Opposite signs for the eigenvectors are also obtained if we analyze a 2×2 correlation matrix, as long as interpolator $\chi_1^{(8)}$ is used together with either $\chi_1^{(6)}$ or $\chi_1^{(7)}$.

Let us next vary t_0 as suggested in Ref. [10], shown to lead to an improvement in the determination of the ground state by successfully suppressing excited state

contamination for certain mesonic systems. In Fig. 7 we show results obtained at fixed $t_0/a = 1$ as well as results obtained by varying t_0 using *basis A*. Within the statistical accuracy of our analysis, we see consistent results for the three values of $t_0/a = 1, 3, \text{ and } 5$ considered. Furthermore, we allow t_0 to vary for every value of t and in particular we apply the condition $t_0 \geq t/2$ as suggested in Ref. [10]. We show results for the ground and first excited states in the positive parity channel for the case $t_0 = t/2$, where we observe no change in the plateau range within the present statistics. For these nucleon states and within the present accuracy, this analysis does not show an improvement, a result that is also valid for the variational *basis B*. Our conclusion is that for the low-lying nucleon spectrum, where the energy gap is not particularly small, the variation of t_0 that has been shown in Ref. [10] to reduce the systematic error is not observed here at least within the limitation of our statistics. Keeping $t_0 \geq t/2$ comes at the cost of increased statistical uncertainty. In our case, this increase is large and we find that the highest overall precision is obtained by keeping $t_0/a = 1$.

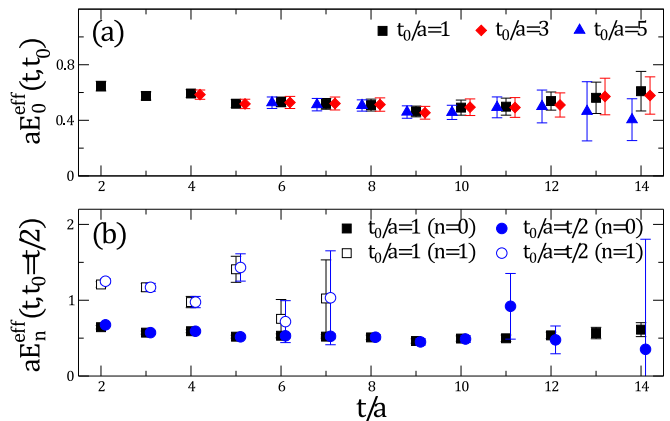


FIG. 7. (a) The effective mass for the ground state for various choices of t_0 . Results are shown for the 3×3 GEVP with the most smeared interpolating fields within *basis A*. (b) The effective mass for the ground and first excited states with a fixed value for t_0 (squares) and with the condition $t_0 = t/2$ (circles) for the ground (filled symbols) and first excited state (open symbols). Values have been slightly shifted in time in order to aid the comparison.

From the above analysis it is clear that the merit of the variational approach lies in the extraction of excited states, whereas the ground state is equally well obtained using just a single smeared interpolating function, in our case either $\chi_1^{(7)}$ or $\chi_1^{(8)}$. In Fig. 8 we analyze the 5×5 GEVP of *basis A* to extract the nucleon spectrum. Despite the low statistics used in this first examination we are able to obtain effective mass plateaus $m_{\text{eff}}(n)$ for the ground-state ($n = 0$) and the three excited states ($n = 1, n = 2$ and $n = 3$), as has already been done in other works [11, 23]. Fig. 8 corroborates the previous observation that including a heavily smeared interpolating field in the basis produces an excited state with a lower en-

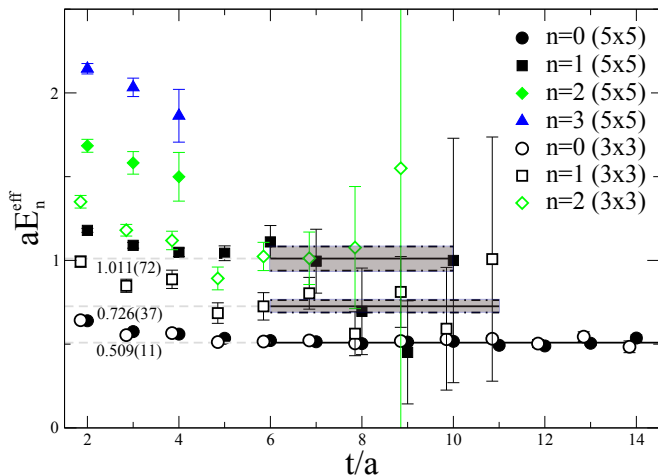


FIG. 8. The spectrum when using $\chi_1^{(i)}$ at $\beta=3.9$, $a\mu = 0.004$ ($m_\pi \sim 308$ MeV) on a $32^3 \times 64$ lattice. For the 5×5 GEVP we use 150 configurations and *basis A*. For the 3×3 GEVP we use 250 configurations with *basis B*. The solid lines and bands show the fitted effective mass and jackknife error for the first excited state obtained from the two different GEVPs.

ergy. Although increasing the level of smearing is essential for the positive parity excited states, this is not the case when the negative parity channel is considered, This issue will be discussed further in the following section.

B. Combining both χ_1 and χ_2

In the preceding subsection we used a variational basis constructed from different smearing levels of the χ_1 interpolating field. In this section, we extend the investigation by combining both $\chi_1^{(i)}$ and $\chi_2^{(i)}$ each with two different smearing levels resulting in a 4×4 correlation matrix.

For the positive parity channel we consider two different smearing levels including the heavily smeared one that was found to give a lower excited state energy, namely we consider $n_s=50$ and $n_s = 180$ with $\alpha=4.0$ or correspondingly interpolating fields $\chi_a^{(7)}$ and $\chi_a^{(8)}$ with $a = 1, 2$. In Fig. 9 we compare the results for the effective masses of the ground and first excited state in the positive parity channel extracted using this 4×4 basis with those extracted from *basis B* of the previous section (see Fig. 8). The effective mass plateaus are statistically equivalent for both basis sets.

It is evident from the preceding analysis that the first excited state can be obtained from the 2×2 GEVP using $C_{1_i 1_j}$ with $i, j = 7, 8$, or equivalently from the 4×4 GEVP using $C_{a_i b_j}$ with $a, b = 1, 2$ and $i, j = 7, 8$, a result that we will use in order to further examine the first excited state for other ensembles. We note that in both cases we use two different smearing levels.

Let us now examine the negative parity states. We first note that the negative parity interpolating operator

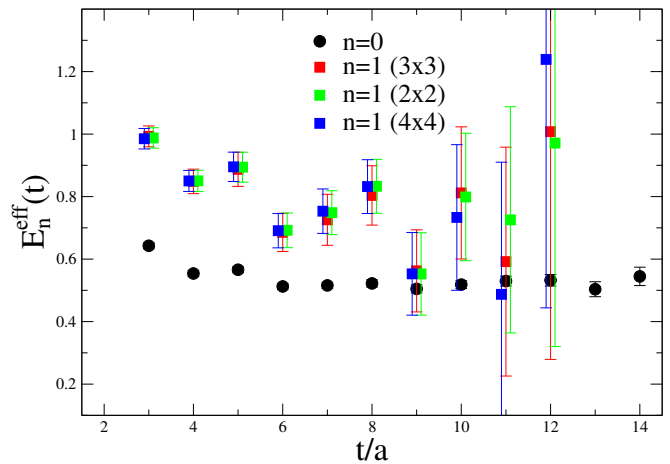


FIG. 9. The effective mass for the ground and first excited states for the positive parity channel for $\beta=3.9$, $a\mu = 0.004$ on a $32^3 \times 64$ lattice. The 3×3 system is constructed using *basis B*; The 2×2 system corresponds to $C_{1_i 1_j}$ with $i, j = 7, 8$ and the 4×4 corresponds to $C_{a_i b_j}$ with $a, b = 1, 2$ and $i, j = 7, 8$. 250 configurations are used.

in Eq. 2 has a non-zero overlap with the two particle S-wave state that consists of a nucleon and a pion. At the physical point, this state has lower energy than the negative parity nucleon. To know *a priori* at which pion mass, the mass of the negative parity nucleon and the mass of the πN state cross requires knowledge of the pion mass dependence of the negative parity nucleon.

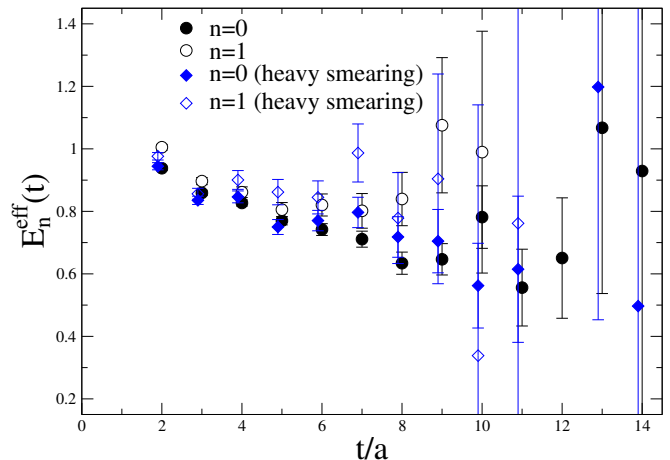


FIG. 10. The nucleon ground (filled symbols) and first excited states (open symbols) in the negative parity channel, evaluated via a 4×4 GEVP using two different basis sets: $\{\chi_1^{(1)}, \chi_1^{(5)}, \chi_2^{(1)}, \chi_2^{(5)}\}$ (black circles) and the set $\{\chi_1^{(7)}, \chi_1^{(8)}, \chi_2^{(7)}, \chi_2^{(8)}\}$ (blue diamonds). 250 configurations were used for this test.

To explore the best variational basis for the negative parity channel we carry out a similar analysis as with the positive parity channel. We use two different bases each leading to a 4×4 correlation matrix using both $\chi_1^{(i)}$

and $\chi_2^{(i)}$. In the one set we use $i = 1, 5$ while in the other $i = 7, 8$ i.e. the latter includes the heavily smeared interpolating fields. As is illustrated in Fig. 10, including the heavily smeared interpolator yields consistent results but with increased statistical error. In Fig. 11, we show the ground and first excited states obtained from a 4×4 and 2×2 GEVP. As in the case of Fig. 10, the 4×4 correlation matrix is constructed using the basis $\chi_a^{(i)}$ with $a = 1, 2$ and $i = 1, 5$, while the 2×2 using $\{\chi_1^{(5)}, \chi_2^{(5)}\}$ (note that the basis $\{\chi_1^{(7)}, \chi_2^{(7)}\}$ yield equivalent results). As can be seen, the two basis yield results for the ground and first excited states that are statistically equivalent.

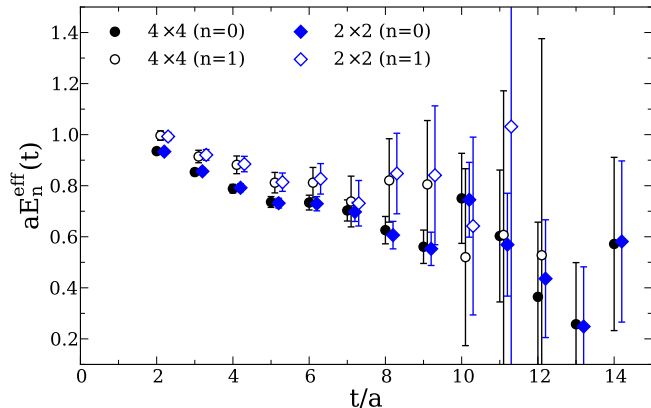


FIG. 11. The nucleon ground (filled symbols) and first excited states (open symbols) in the negative parity channel, evaluated using a 4×4 correlation matrix (black circles) and a 2×2 correlation matrix (blue diamonds). The variational bases used are $\chi_a^{(i)}$, $a = 1, 2$ and $i = 1, 5$ and $\{\chi_1^{(5)}, \chi_2^{(5)}\}$. 250 configurations were used for this analysis.

Having verified that the 2×2 correlation matrix yields the same energies for the ground and first excited states of the negative parity as the 4×4 correlation matrix does, from here on, we will use the 2×2 basis to resolve the ground and first excited negative parity states for all other pion masses. Knowing which one of these is the multi-particle state would require investigation of the dependence of the two energy levels on the lattice volume, which is beyond the resources available to us for this work. Therefore, we compare the two energy states with the sum of the nucleon and pion mass, and from this infer which is the negative parity nucleon state. Further examples of the effective masses extracted from the 2×2 correlation matrix are given in Figs. 12 and 13, discussed in the following section.

IV. THE LOW-LYING NUCLEON SPECTRUM

In the previous section, we have shown that if we are interested in the first excited positive parity states of the nucleon the variational analysis using *basis B* is preferable to *basis A*. Furthermore, we showed that the inter-

polating fields $\chi_a^{(i)}$ with $a = 1, 2$ and $i = 7, 8$ suffice to determine the two lowest state. Thus we construct a 4×4 correlation matrix, with variational basis consisting of χ_1 and χ_2 with two different smearing levels, one yielding a small rms radius and one a large one. The negative parity states were shown to be best extracted from a 2×2 correlation matrix analysis, with a single level of smearing using both interpolating operators (i.e. $\chi_1^{(7)}$ and $\chi_2^{(7)}$). We also note that results presented from here on have been obtained with the statistics listed in Table I.

In Figs. 12 and 13 we show the effective masses for both positive and negative parity states, for a twisted mass ensemble and for the Clover ensemble analyzed in this work. As can be seen, a plateau region can be identified for all states.

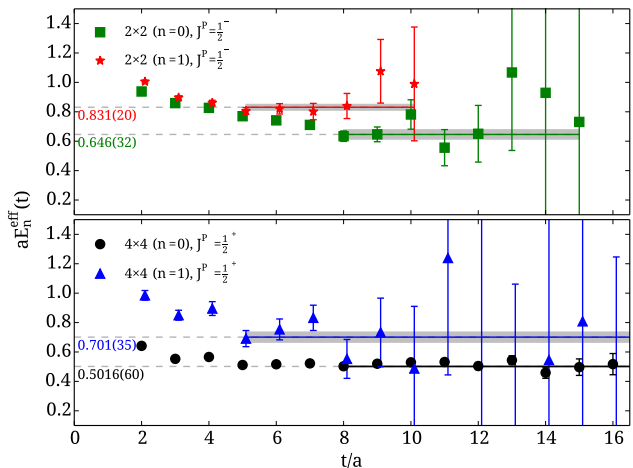


FIG. 12. The effective masses of the two lowest lying nucleon states for the negative (upper panel) and positive (lower panel) states for the twisted mass ensemble with $\beta=3.9$, $a\mu = 0.004$ and volume $32^3 \times 64$. For the positive parity states we use a 4×4 correlation matrix with $\{\chi_1^{(7)}, \chi_1^{(8)}, \chi_2^{(7)}, \chi_2^{(8)}\}$, while for the negative parity states we use a 2×2 correlation matrix with $\chi_1^{(5)}$ and $\chi_2^{(5)}$ as explained in the text.

The results for all of the ensembles of Table I and the single Clover ensemble are displayed in Fig. 14. For the nucleon mass we apply continuum chiral perturbation theory to extrapolate lattice results to the physical pion mass, omitting the Clover point from the fit. We use SU(2) heavy baryon chiral perturbation theory to $\mathcal{O}(p^3)$ given by

$$m_N(m_\pi) = m_N^{(0)} - 4c_N^{(1)} m_\pi^2 - \frac{3g_A^2}{16\pi f_\pi^2} m_\pi^3. \quad (7)$$

Since the lattice spacing was fixed using the nucleon mass for the twisted mass ensembles it is no surprise that the curve passes through the physical value. Since the Clover point was not included in the fit the fact that it lies on the curve provides a consistency check for our procedure. In the figure we also show a curve obtained by adding the pion mass to the nucleon mass. As can be seen, for all

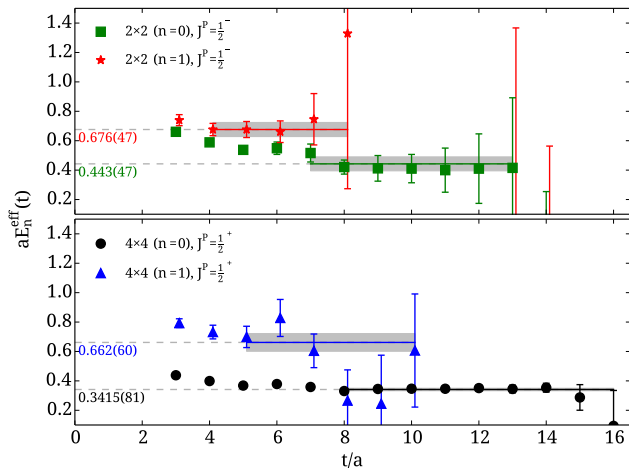


FIG. 13. The effective masses of the two lowest lying nucleon states for the negative (upper panel) and positive (lower panel) states for the Clover ensemble. The notation is the same as in Fig. 12

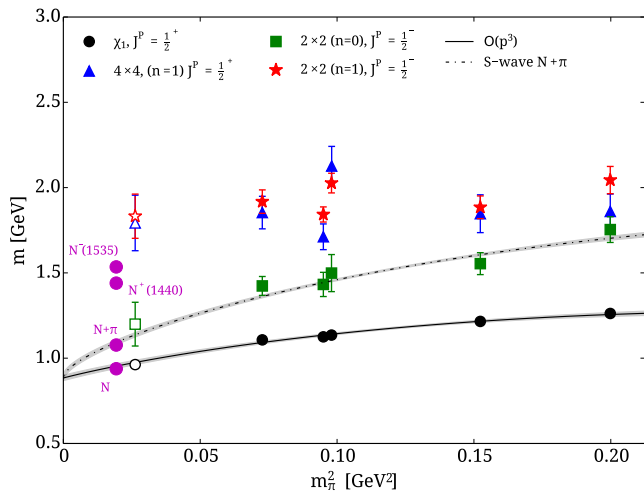


FIG. 14. The first two positive and negative parity states measured on all gauge ensembles considered in this work. The twisted mass ensembles are plotted with filled symbols, while the results from the single Clover ensemble are denoted with the open symbols. We show chiral extrapolations for the nucleon ground state to $\mathcal{O}(p^3)$ as in Eq. 7, omitting the Clover point from the fit. The dashed line is a result of adding the pion mass to the $\mathcal{O}(p^3)$ curve. Physical masses for the different states are indicated by the magenta filled circles.

pion masses considered here, the negative parity ground state is consistent with the mass of the pion plus nucleon, indicating that this is the two particle πN state in an S-wave configuration. We also observe that the first excited states in the positive and negative channels remain close together for all pion masses.

In Figs. 15 and 16 we compare the results of this work with three other calculations available in the literature. Namely, we compare with the results obtained

using a Clover improved fermion action by the CSSM collaboration [24] with $a \simeq 0.09$ fm, a calculation using anisotropic Clover lattices by the Hadron Spectrum Collaboration [25] with spatial lattice spacing $a_s = 0.123$ fm and a calculation using the Chirally Improved Dirac Operator by the BGR collaboration [20] and lattice spacings between 0.13 and 0.14 fm. We note that the lattice spacings for the two latter calculations are notably larger than those used in this work arising issues about cut-off effects.

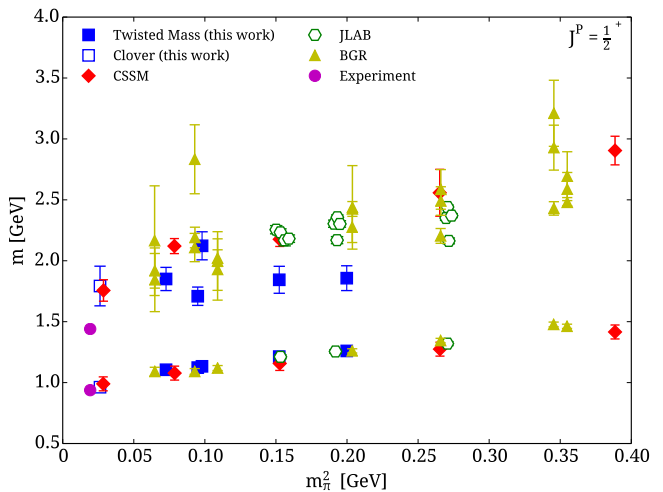


FIG. 15. The positive parity states of this work (filled and open squares) compared with results from other groups, that include a $N_f = 2 + 1$ Clover improved fermion calculation by the CSSM collaboration [24] (red diamonds), a calculation using anisotropic clover lattices by the Hadron Spectrum Collaboration [25] (open hexagons) and a calculation using the Chirally Improved Dirac Operator by the Bern-Graz-Regensburg (BGR) collaboration [20] (yellow triangles).

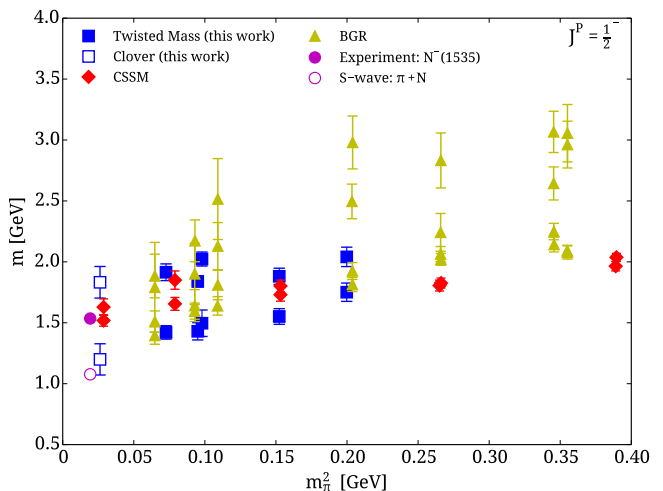


FIG. 16. The negative parity states of this work compared with calculations from other groups. The CSSM results are from [26], while the rest of the notation is as in Fig. 15.

The first observation is that all lattice results are in reasonable agreement for the ground state energies of both parity channels. The second major observation is that our data for the first excited state of the nucleon in the positive parity channel, although consistent at near physical pion mass with the other lattice calculation at similar pion mass, namely that from the CSSM Collaboration, is still higher than the experimentally measured mass for the Roper. Given that our lattice volume is comparable to that of Ref. [24] volume effects can be responsible for the larger values. In the negative parity channel our results are consistent with the ones from the BGR collaboration. We can clearly see that for all pion masses considered the negative parity ground state is consistent with a πN state in an S-wave. To the statistical accuracy available to us, the first excited negative parity state appears to be converging to $N^-(1535)$, however the errors are too large to draw concrete conclusions. Overall, the early loss of signals seen in the plateaus of the excited states shown in Figs. 12 and 13 indicates that a high statistics calculation of these quantities is merited using e.g. recently developed noise reduction techniques [27].

V. CONCLUSIONS

In this work we apply the variational method to investigate the excited states of the nucleon. Two sets of variational bases are used and the analysis of the resulting GEVP was performed using the standard approach of fixing t_0 as well as by varying t_0 such that $t_0 \geq t/2$ as advocated in Ref. [10]. Within the current statistical accuracy, we found that for the nucleon excited states no observable improvement is obtained as compared to fixing t_0 . Limiting ourselves to the first excited state of the nucleon in the positive parity channel requires a combination of one broadly and one narrowly smeared interpolating field. Including both χ_1 and χ_2 yields a 4×4 correlation matrix, which we use to extract results in the positive parity channel for a number of $N_f = 2$

twisted mass fermion ensembles. Besides the twisted mass fermion ensembles we use in addition an $N_f = 2$ clover fermion ensemble with pion mass almost equal to the physical value. At this lightest pion mass of 160 MeV we find an excited state, which is still higher than the Roper but consistent with another calculation at similar pion mass from the CSSM collaboration. We do not observe a strong pion mass dependence and the higher value may be due to finite volume effects, which must be further investigated. In the negative parity channel we obtain results that reveal the πN scattering state and an excited state, which at $m_\pi = 160$ MeV is still higher than the physical value of N^- . It is clear from this analysis that extracting the excited states is still a challenge and more work is needed to understand the low-lying spectrum of the nucleon.

ACKNOWLEDGMENTS

For the numerical calculations, we have used the Cy-Tera facility of the Cyprus Institute under the Cy-Tera first access call (Project No. lspro113s1) and third access call (Project No. lsprob115s1). The Cy-Tera project is funded by the Cyprus Research Promotion Foundation under Contract No. NEA YΠOΔOMH/ΣΤΡΑΤΗ/0308/31. In addition, this work was granted access to the HPC system “Lindgren” of KTH Stockholm made available within the Distributed European Computing Initiative by the PRACE-2IP receiving funding from the European Community’s Seventh Framework Programme (FP7/2007-2013) under Grant No. RI-283493. We thank the staff members of these sites for their kind and sustained support. This work is supported in part by the Cyprus Research Promotion Foundation under Contract No. KY-/0310/02/, the Research Executive Agency of the European Union under Grant No. PITN-GA-2009-238353 (ITN STRONGnet) and the FP7 infrastructures-2011-1 project Hadron-Physics3 under Grant No. 283286.

-
- [1] S. Durr et al., *Science* **322**, 1224 (2008).
 - [2] C. Alexandrou et al. (European Twisted Mass Collaboration), *Phys. Rev.* **D78**, 014509 (2008), 0803.3190.
 - [3] C. Michael and I. Teasdale, *Nucl.Phys.* **B215**, 433 (1983).
 - [4] S. Basak, R. Edwards, G. Fleming, K. Juge, A. Lichtl, et al., *Phys.Rev.* **D76**, 074504 (2007), 0709.0008.
 - [5] C. Gattringer, L. Y. Glozman, C. Lang, D. Mohler, and S. Prelovsek, *Phys.Rev.* **D78**, 034501 (2008), 0802.2020.
 - [6] C. Gattringer, C. Hagen, C. Lang, M. Limmer, D. Mohler, et al., *Phys.Rev.* **D79**, 054501 (2009), 0812.1681.
 - [7] M. Mahbub, A. O. Cais, W. Kamleh, D. B. Leinweber, and A. G. Williams, *Phys.Rev.* **D82**, 094504 (2010), 1004.5455.
 - [8] J. Bulava, R. Edwards, E. Engelson, B. Joo, H.-W. Lin, et al., *Phys.Rev.* **D82**, 014507 (2010), 1004.5072.
 - [9] M. Luscher and U. Wolff, *Nucl.Phys.* **B339**, 222 (1990).
 - [10] B. Blossier, M. Della Morte, G. von Hippel, T. Mendes, and R. Sommer, *JHEP* **0904**, 094 (2009), 0902.1265.
 - [11] M. S. Mahbub, W. Kamleh, D. B. Leinweber, P. J. Moran, and A. G. Williams (CSSM Lattice collaboration), *Phys.Lett.* **B707**, 389 (2012), 1011.5724.
 - [12] D. S. Roberts, W. Kamleh, and D. B. Leinweber, *PoS LATTICE2012*, 261 (2012).
 - [13] C. Alexandrou et al. (ETM Collaboration), *Phys. Rev.* **D80**, 114503 (2009), 0910.2419.
 - [14] C. Urbach (European Twisted Mass Collaboration), *PoS LAT2007*, 022 (2007), 0710.1517.
 - [15] G. Bali, P. Bruns, S. Collins, M. Deka, B. Glasle, et al., *Nucl.Phys.* **B866**, 1 (2013), 1206.7034.
 - [16] M. Albanese et al. (APE Collaboration), *Phys.Lett.* **B192**, 163 (1987).

- [17] S. Durr, G. Koutsou, and T. Lippert, *Phys.Rev.* **D86**, 114514 (2012), 1208.6270.
- [18] F. X. Lee and D. B. Leinweber, *Nucl.Phys.Proc.Suppl.* **73**, 258 (1999), hep-lat/9809095.
- [19] B. J. Menadue, W. Kamleh, D. B. Leinweber, M. S. Mahbub, and B. J. Owen (2013), 1302.4152.
- [20] G. P. Engel, C. Lang, D. Mohler, and A. Schfer (BGR), *Phys.Rev.* **D87**, 074504 (2013), 1301.4318.
- [21] S. Gusken, *Nucl. Phys. Proc. Suppl.* **17**, 361 (1990).
- [22] C. Alexandrou, S. Gusken, F. Jegerlehner, K. Schilling, and R. Sommer, *Nucl. Phys.* **B414**, 815 (1994), hep-lat/9211042.
- [23] M. Mahbub, A. O. Cais, W. Kamleh, B. G. Lasscock, D. B. Leinweber, et al., *Phys.Lett.* **B679**, 418 (2009), 0906.5433.
- [24] M. Mahbub, W. Kamleh, D. Leinweber, P. Moran, and A. Williams, *AIP Conf.Proc.* **1441**, 293 (2012).
- [25] R. G. Edwards, J. J. Dudek, D. G. Richards, and S. J. Wallace, *Phys.Rev.* **D84**, 074508 (2011), 1104.5152.
- [26] M. S. Mahbub, W. Kamleh, D. B. Leinweber, P. J. Moran, and A. G. Williams, *Phys.Rev.* **D87**, 094506 (2013), 1302.2987.
- [27] T. Blum, T. Izubuchi, and E. Shintani, *Phys.Rev.* **D88**, 094503 (2013), 1208.4349.